

Original Article

Cite this article: Seckeler MD, Boe BA, Barber BJ, Berman DP, and Armstrong AK (2021) Use of rotational angiography in congenital cardiac catheterisations to generate three-dimensional-printed models. *Cardiology in the Young* 31: 1407–1411. doi: [10.1017/S1047951121000275](https://doi.org/10.1017/S1047951121000275)

Received: 5 August 2020
Accepted: 11 January 2021
First published online: 18 February 2021

Keywords:

Three-dimensional printing; congenital heart disease; cardiac catheterisation; tetralogy of Fallot

Author for correspondence:

Dr M. Seckeler, MD, MSc, Department of Pediatrics (Cardiology), University of Arizona, 1501 N. Campbell Ave, PO Box 245073, Tucson, AZ 85724, USA. Tel: +520 626 5585; Fax: +520 626 6571. E-mail: mseckeler@peds.arizona.edu

The rotational angiograms were performed at the Nationwide Children's Hospital and Banner University Medical Center – Tucson/University of Arizona. The three-dimensional model generation and printing were performed at the Banner University Medical Center – Tucson/University of Arizona.

Use of rotational angiography in congenital cardiac catheterisations to generate three-dimensional-printed models

Michael D. Seckeler¹ , Brian A. Boe², Brent J. Barber¹, Darren P. Berman² and Aimee K. Armstrong²

¹University of Arizona, Department of Pediatrics (Cardiology), Tucson, AZ, USA and ²The Heart Center, Nationwide Children's Hospital, Columbus, OH, USA

Abstract

Background: Three-dimensional printing is increasingly utilised for congenital heart defect procedural planning. CT or MR datasets are typically used for printing, but similar datasets can be obtained from three-dimensional rotational angiography. We sought to assess the feasibility and accuracy of printing three-dimensional models of CHD from rotational angiography datasets. **Methods:** Retrospective review of CHD catheterisations using rotational angiography was performed, and patient and procedural details were collected. Imaging data from rotational angiography were segmented, cleaned, and printed with polylactic acid on a Dremel® 3D Idea Builder (Dremel, Mount Prospect, IL, USA). Printing time and materials' costs were captured. CT scans of printed models were compared objectively to the original virtual models. Two independent, non-interventional paediatric cardiologists provided subjective ratings of the quality and accuracy of the printed models. **Results:** Rotational angiography data from 15 catheterisations on vascular structures were printed. Median print time was 3.83 hours, and material costs were \$2.84. The CT scans of the printed models highly matched with the original digital models (root mean square for Hausdorff distance 0.013 ± 0.003 mesh units). Independent reviewers correctly described 80 and 87% of the models ($p = 0.334$) and reported high quality and accuracy (5 versus 5, $p = \text{NS}$; $\kappa = 0.615$). **Conclusion:** Imaging data from rotational angiography can be converted into accurate three-dimensional-printed models of CHD. The cost of printing the models was negligible, but the print time was prohibitive for real-time use. As the speed of three-dimensional printing technology increases, novel future applications may allow for printing patient-specific devices based on rotational angiography datasets.

Since three-dimensional printing technology was first described by Charles Hull in 1986,¹ technological advances have led to increased use in the medical field, including for education,^{2,3} procedural planning,^{4,5} and device development.⁶ Typical datasets for three-dimensional model generation come from computed tomography or magnetic resonance scans that are segmented to highlight the regions of interest, converted to stereolithographic format, and printed. Three-dimensional rotational angiography is a newer imaging modality performed in the cardiac catheterisation laboratory and produces a three-dimensional dataset that can be used for the virtual reconstruction of complex structures. It was initially used in neurovascular interventions⁷ and was first used in a congenital cardiac catheterisation in 2007.⁸ With improved image processing and the ability to overlay three-dimensional reconstructions onto standard fluoroscopic imaging, rotational angiography use has continued to increase for diagnostic^{9–15} and interventional^{16–25} congenital cardiac catheterisation.

Rotational angiography imaging provides datasets similar to other advanced imaging modalities for the creation of highly detailed, patient-specific three-dimensional virtual models. In addition, rotational angiography may be more advantageous than multi-slice CT scans, as the imaging is focused on the area of interest, generating less radiation exposure.²⁶ There are few publications detailing the use of rotational angiography datasets of CHD to generate three-dimensional-printed models.^{19,27} The purpose of this study was to create three-dimensional-printed models from rotational angiography datasets of CHD and assess the quality (both objectively and subjectively) of the models produced.

Materials and methods

After approval from the Institutional Review Boards of the University of Arizona and Nationwide Children's Hospital, congenital catheterisations that used rotational angiography from January, 2017 to March, 2018 were retrospectively identified. Catheterisations were performed in Toshiba and Philips laboratories. Rapid ventricular pacing, contrast concentration,

© The Author(s), 2021. Published by Cambridge University Press. This is an Open Access article, distributed under the terms of the Creative Commons Attribution licence (<https://creativecommons.org/licenses/by/4.0/>), which permits unrestricted re-use, distribution, and reproduction in any medium, provided the original work is properly cited.

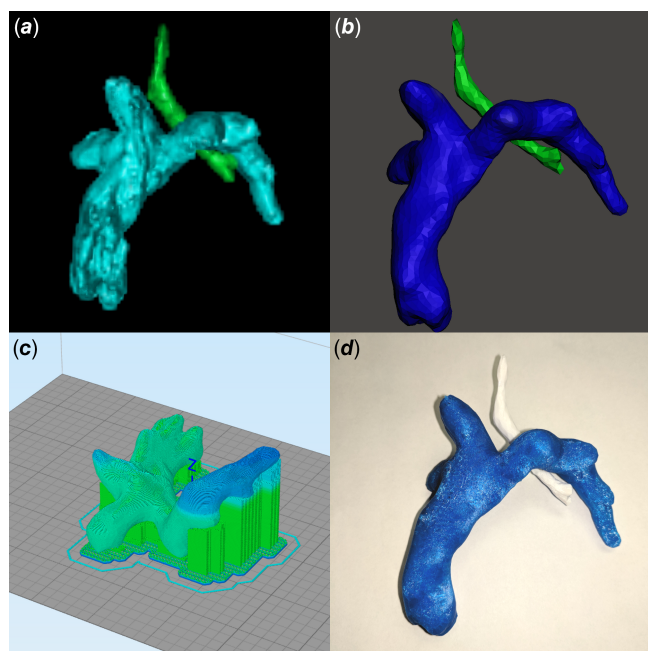


Figure 1. Generation of a three-dimensional-printed model from three-dimensional rotational angiography data. (a) Digital Imaging and Communications in Medicine data are first segmented to define the anatomy of interest (Fontan circuit in cyan, trachea in green). (b) The model is cleaned (Fontan circuit in blue, trachea in green). (c) The model is prepared for printing. (d) Final three-dimensional-printed model (Fontan circuit in blue, trachea in white).

and contrast volume were based on standard practice and operator preference. Cases were chosen to reflect various CHD anatomies. Digital Imaging and Communications in Medicine data were segmented using a semi-automated process with Philips IntelliSpace Portal (Philips Medical Systems, The Netherlands), cleaned using Autodesk® Meshmixer™ (Autodesk, Inc., San Rafael, CA, USA), prepared for printing using Simplify3D® version 4.0.0 (Simplify3D Software, Cincinnati, OH, USA), and printed with polylactic acid on a Dremel® 3D Idea Builder (Dremel, Mount Prospect, IL, USA, list price \$1299; Fig 1a–d). All segmentations, model generations, and printings were performed by a single user (MDS) who has personally generated over 250 three-dimensional-printed models of CHD. Data collected included patient demographics, diagnosis, and contrast concentration and volume used for the rotational angiography. Three-dimensional printing time and materials' costs were also collected.

Printed three-dimensional models were objectively assessed using a method described for three-dimensional printing of livers.²⁸ The printed models were imaged using a Siemens Inveon uCT scanner (Siemens Medical Solutions USA, Inc., Malvern, PA, USA). A total of 360 projections were acquired in a full rotation, using low magnification with a 4×4 binning. The camera was set in rat mode with a transaxial field of view of 3072 px (81.02 mm), and axial scan length was set at 128 mm, which requires three bed positions and uses a 31.52% field of view overlap for reconstruction. Exposure settings were 80 kV, with 500 μA current and an acquisition time of 250 ms. Image reconstruction was done using a Feldkamp algorithm, a Shepp–Logan filter, slight noise reduction, and twofold downsampling. Digital Imaging and Communications in Medicine images from the CT were segmented using Philips IntelliSpace Portal and were compared to the original digital models using MeshLab version

Table 1. Patient demographics and cardiac diagnoses. Data are shown as n (%) or median (interquartile range)

Age (years)	5.8 (0.7, 14.4)
Weight (kg)	17.1 (10, 41.7)
Diagnosis	
Aortic coarctation/recoarctation/stent placement	3 (20)
Single ventricle s/p SCPC or TCPC	3 (20)
Hypoplastic left heart syndrome s/p stage 1 palliation	2 (13)
Tetralogy of Fallot/pulmonary atresia/MAPCAs	2 (13)
Branch PA stenosis	2 (13)
Coronary artery fistula	1 (7)
RV-PA conduit stenosis	1 (7)
Superior caval vein stenosis	1 (7)

MAPCAs = major aortopulmonary collateral arteries; PA = pulmonary artery; RV-PA = right ventricle to pulmonary artery; SCPC = superior cavopulmonary connection; TCPC = total cavopulmonary connection

Table 2. Image acquisition details and costs and times for three-dimensional model printing. Data are shown as n (%) or median (interquartile range)

Rotational angiography details	
Rapid pacing (n (%))	10 (67)
Contrast concentration (%)	60 (50, 100)
Contrast volume (ml/kg)	1.55 (1.03, 1.91)
Printing details	
Filament weight (g)	61.84 (25.58, 86.7)
Print time (hours)	3.83 (3.35, 7.02)
Materials' cost (US\$)	2.84 (1.43, 3.99)

2016.12 (Visual Computing Laboratory, Pisa, Italy). Hausdorff distances were calculated with vertex samples, using at least 100,000 samples, and the root mean square of the difference was calculated for each model comparison.²⁹ Distances were reported as “mesh units”, not absolute measures, and the closer the root mean square was to 0, the more similar the models.

For a subjective assessment of the printed models, two blinded, independent, non-interventional paediatric cardiologists provided descriptions of the anatomy and any interventions (e.g., hypoplastic left heart syndrome after Norwood reconstruction with a modified Blalock–Taussig–Thomas shunt) based on the three-dimensional-printed models. In addition, they provided a subjective rating (1–5) of quality and accuracy of the three-dimensional-printed models as compared to the original digital models.

Data were compared using Mann–Whitney U test, χ^2 , and κ for agreement, as appropriate. A p-value <0.05 was considered statistically significant.

Results

Data from 15 rotational angiograms were three-dimensional printed. Patient characteristics and diagnoses are shown in Table 1. Details of image acquisition and three-dimensional printing are shown in Table 2. Because of the focal application of

Table 3. Summary of anatomic descriptions of underlying cardiac defects and interventions along with descriptions provided by the independent reviewers. There were two models of complex, abnormal branch pulmonary arteries that were incorrectly identified by both reviewers. Of note, the full cardiac diagnoses are provided for completeness, but the majority of the three-dimensional-printed models did not include intracardiac anatomy, so the description of this was not expected of the reviewers

Model	Anatomy	Reviewer #1	Reviewer #2
1	Pulmonary atresia with VSD and MAPCAs	Pulmonary atresia with MAPCAs with a large plexus of vessels off the descending aorta	Pulmonary atresia with MAPCAs
2	DORV/TGA/mitral atresia s/p TCPC with left PA stenosis	SCPC with proximal left PA stenosis; left PA in close proximity to left bronchus	SCPC with left PA stenosis
3	Shone's complex with hypoplastic aortic arch s/p stent placement	Hypoplastic transverse aortic arch s/p stent placement	Diffuse aortic arch hypoplasia
4	L-TGA, pulmonary atresia, VSD s/p SCPC with left PA hypoplasia	SCPC with right PA larger than left	SCPC with diffuse left PA hypoplasia
5	HLHS s/p hybrid stage 1 palliation and SCPC now with recoarctation	HLHS s/p stage 1 and SCPC palliations, probable aortic coarctation	S/p Damus–Kaye–Stansel aortic reconstruction, s/p SCPC, recoarctation of the aorta
6	Large coronary artery fistula from circumflex to coronary sinus	Massive left coronary artery, suspect fistula off left coronary artery	Left coronary artery fistula
7	Type B interrupted aortic arch s/p stent for recoarctation	Narrow transverse aortic arch s/p probable stent placement, bovine arch	Coarctation of the aorta s/p stent, bovine arch
8	Truncus arteriosus s/p repair with RV-PA conduit with distal conduit stenosis	Mild right PA stenosis	Left PA stenosis
9	Unbalanced AVSD, TGA, pulmonary atresia s/p PA unifocalisation, and BTT shunt	Single ventricle s/p BTT shunt off of innominate artery	BTT shunt versus PDA from left subclavian artery supplying pulmonary arteries
10	HLHS s/p hybrid stage 1, recoarctation	Hypoplastic left heart syndrome with aortic valve atresia, stented PDA, PA bands	S/p hybrid stage 1 palliation (PDA stent, bilateral PA bands)
11	DCRV, VSD, PAPVR s/p VSD closure/muscle resection, now with left PA stenosis	Main and branch pulmonary arteries with dilation of PA sinuses	S/p SCPC
12	Truncus arteriosus s/p repair, complex bilateral proximal branch PA stenoses	Tortuous takeoff of bilateral branch pulmonary arteries without a sling	Left PA sling
13	DORV/interrupted aortic arch s/p complete repair, including arch reconstruction, now with recoarctation	Hypoplastic transverse aortic arch with abnormal ascending aorta and narrowing between carotid and left subclavian artery	Transverse arch narrowing
14	PAPVR s/p Warden procedure with SVC stenosis	SVC into right atrium	SVC narrowing
15	Pulmonary atresia/MAPCAs s/p multiple aortopulmonary shunts	Dilated ascending aorta with multiple collaterals	Pulmonary atresia with MAPCAs

AVSD = atrioventricular septal defect; BTT = Blalock–Taussig–Thomas; DCRV = double chamber right ventricle; DORV = double outlet right ventricle; HLHS = hypoplastic left heart syndrome; MAPCAs = major aortopulmonary collateral arteries; PA = pulmonary artery; PAPVR = partial anomalous pulmonary venous return; PDA = patent ductus arteriosus; RV-PA = right ventricle to pulmonary artery; SCPC = superior cavopulmonary connection; SVC = superior caval vein; TCPC = total cavopulmonary connection; TGA = transposition of the great arteries; VSD = ventricular septal defect

contrast to the structure(s) of interest, initial segmentation time was less than 10 minutes per model, which was half the typical time for segmentation of similar anatomy from CT or MR dataset (MDS, personal experience). The median time to print the three-dimensional models was 3.83 hours (IQR 3.35, 7.02 hours), with a material cost of \$2.84 per model. Print time and material cost were affected by model size and complexity. All models were of vascular structures (aorta, main/branch pulmonary arteries, superior/total cavopulmonary connections, coronary artery fistula, superior caval vein). There was very high agreement between the original digital reconstructions and those generated from CT scans of the printed models (root mean square for Hausdorff distance 0.013 ± 0.003 mesh units). Model descriptions by the independent reviewers are shown in Table 3. They correctly described the anatomy and interventions for 80 and 87% of the models ($p = 0.334$) and rated the quality and accuracy of the models high

with a substantial agreement (5 versus 5, $p = \text{NS}$; $\kappa = 0.615$). Two models were incorrectly described by both reviewers.

Discussion

In this series, rotational angiography data from congenital cardiac catheterisations of a variety of defects and surgical palliations were successfully and accurately printed as three-dimensional models. While there are two small prior reports of this technique,^{19,27} we generated models from a wide variety of CHD anomalies and provided objective measures to assess the accuracy of the printed models. There are several potential advantages of using three-dimensional datasets from rotational angiography to generate three-dimensional-printed models.

A valuable clinical application of three-dimensional-printed models from rotational angiography is for surgical planning.

The utility of three-dimensional-printed models from CT and MR datasets for planning the surgical approach for complex CHD has been well documented.³⁰ Many patients with CHD undergo a pre-operative diagnostic cardiac catheterisation to obtain haemodynamic data. Utilisation of rotational angiography data for three-dimensional models minimises the need for additional procedures, radiation, and general anaesthetic exposure. Our findings show that the three-dimensional-printed models from rotational angiography datasets are high quality, accurate, and should be acceptable for surgical planning.

Another use for three-dimensional-printed models generated from rotational angiography is for educational purposes. Additional advanced imaging is not always obtained for patients who undergo cardiac catheterisations, but there is a value in understanding their complex anatomy. If rotational angiography datasets are being obtained as part of routine care, then these existing datasets can be used to generate libraries of CHD for trainees, such as has been done for interventional radiology, neuroradiology, and structural heart disease.^{5,31} Many interventionalists use the 2D angiography performed during procedures to educate patients and families, but recent studies have shown three-dimensional models to be more effective for family understanding in pre-procedure meetings for cardiac and neurosurgical procedures.^{32,33} The additional time needed to generate three-dimensional virtual models from rotational angiography for this purpose is minimal, and it is feasible to three-dimensional print a small model after the procedure and before hospital discharge. As three-dimensional printing technology becomes faster, it is conceivable that printed models of pre- and post-intervention anatomy could be generated during the catheterisation procedure. These models would provide families a better understanding of the indications and outcomes of an intervention.

Looking beyond the current limitations of our technology, there is a much more practical and exciting potential use of real-time three-dimensional printing. A major challenge for transcatheter interventions in infants and children with CHD is the need to modify existing equipment, such as stents, to fit their unique anatomy.³⁴ The use of three-dimensional printing to create custom stents for a patient has been proposed.³⁵ As three-dimensional printing of metals becomes faster, it is conceivable that a custom stent could be “designed” using a rotational angiography dataset and three-dimensional printed for implantation during the same catheterisation procedure. This would obviate the need for additional imaging and invasive procedures in this fragile population. The application of real-time three-dimensional printing is still futuristic, due to the high complexity and expense of three-dimensional printing metals, in addition to regulatory and safety challenges. Through continued research and development, however, this technology should be obtainable in the future.

While some are hesitant to adopt the use of rotational angiography due to the radiation exposure involved, this concern has not been borne out in studies. In fact, rotational angiography has been found to have a lower radiation dose than standard two-dimensional angiography³⁶ and two-dimensional digital subtraction angiography,²⁶ and the ability to focus the imaging only on the specific anatomy of interest also allow a lower dose than multi-slice CT scans.²⁶ A complete understanding of fluoroscopy equipment and optimisation of the settings to minimise radiation exposure remains key. The combination of cardiac motion and the relatively slow acquisition time of rotational angiography, compared to multi-slice CT scans, limits the ability to visualise intracardiac

structures with current rotational angiography technology. Currently, rotational angiography offers excellent visualisation of vascular structures. Since the majority of angiography for congenital cardiac interventions is for vascular structures (angioplasty, stenting, and vessel embolisation), this is of minimal concern. Further development of rotational angiography technology and techniques will lead to improved imaging of intracardiac structures.

This study is limited by the small numbers and retrospective design. In addition, depending on the institutional experience and available equipment, the model creation and three-dimensional printing times and costs may vary. While there were some limitations in the ability of the reviewers to describe the exact underlying CHD for several of the models, this was not an expected goal of the study, particularly in light of the fact that only part of the anatomy was visualised with the rotational angiography and physically printed for most of the patients. Regardless of these limitations, the data presented provide insight into an intriguing potential future application to further integrate three-dimensional printing into clinical is for patients with CHD.

This proof of concept study has shown that Digital Imaging and Communications in Medicine data from standard rotational angiography can be successfully converted into three-dimensional-printed models for a variety of CHD with excellent accuracy for defining anatomy. The cost of printing the models was negligible, but the time to print is still too long to allow for real-time use of the models. As the speed of three-dimensional printing technology increases, a novel future application of this technique could allow for the printing of patient-specific stents and devices in the catheterisation lab based on rotational angiography datasets.

Acknowledgements. The authors wish to acknowledge and thank Brenda Baggett for her help performing the CT scans of the three-dimensional-printed models. Dr S. received a grant from the Sarver Heart Center Congenital Heart Disease Education Grant and the University of Arizona College of Medicine Vernon, and Virginia Furrow Award for Medical Education Research to establish a three-dimensional printing programme for congenital heart disease at the University of Arizona, but not to directly support the current study.

Financial support. This research received no specific grant from any funding agency, commercial, or not-for-profit sectors.

Conflicts of interest. None.

Ethical standards. The authors assert that all procedures contributing to this work comply with the ethical standards of the relevant national guidelines on human experimentation and with the Helsinki Declaration of 1975, as revised in 2008, and has been approved by the institutional committees of the University of Arizona and Nationwide Children’s Hospital.

Supplementary material. To view supplementary material for this article, please visit <https://doi.org/10.1017/S1047951121000287>.

References

1. Hull CWA. Apparatus for Production of Three-Dimensional Objects by Stereolithography. UVP Inc., San Gabriel, CA, United States, 1986.
2. Jones TW, Seckeler MD. Use of 3D models of vascular rings and slings to improve resident education. *Congenit Heart Dis* 2017; 12: 578–582.
3. White SC, Sedler J, Jones TW, Seckeler M. Utility of three-dimensional models in resident education on simple and complex intracardiac congenital heart defects. *Congenit Heart Dis* 2018; 13: 1045–1049.
4. Frolich AM, Spallek J, Brehmer L, et al. 3D Printing of intracranial aneurysms using fused deposition modeling offers highly accurate replications. *AJNR Am J Neuroradiol* 2016; 37: 120–124.

5. Giannopoulos AA, Steigner ML, George E, et al. Cardiothoracic applications of 3-dimensional Printing. *J Thorac Imaging* 2016; 31: 253–272.
6. Dzian A, Živčák J, Penciak R, Hudák R. Implantation of a 3D-printed titanium sternum in a patient with a sternal tumor. *World J Surg Oncol* 2018; 16: 7.
7. Thron A, Voigt K. Rotational cerebral angiography: procedure and value. *AJNR Am J Neuroradiol* 1983; 4: 289–291.
8. Rigatelli G, Zamboni A, Cardaioli P. Three-dimensional rotational digital angiography in a complicated case of patent ductus arteriosus transcatheter closure. *Catheter Cardiovasc Interv* 2007; 70: 900–903.
9. Panzer J, Taeymans Y, De Wolf D. Three-dimensional rotational angiography of a patient with pulmonary atresia intact septum and coronary fistulas. *Pediatr Cardiol* 2008; 29: 686–687.
10. Glatz AC, Zhu X, Gillespie MJ, Hanna BD, Rome JJ. Use of angiographic CT imaging in the cardiac catheterization laboratory for congenital heart disease. *JACC Cardiovasc Imaging* 2010; 3: 1149–1157.
11. Berman DP, Khan DM, Gutierrez Y, Zahn EM. The use of three-dimensional rotational angiography to assess the pulmonary circulation following cavo-pulmonary connection in patients with single ventricle. *Catheter Cardiovasc Interv* 2012; 80: 922–930.
12. Glockler M, Koch A, Halbfass J, et al. Assessment of cavopulmonary connections by advanced imaging: value of flat-detector computed tomography. *Cardiol Young* 2013; 23: 18–26.
13. Truong UT, Fagan TE, Deterding R, Ing RJ, Fonseca BM. Use of rotational angiography in assessing relationship of the airway to vasculature during cardiac catheterization. *Catheter Cardiovasc Interv* 2015; 86: 1068–1077.
14. Borik S, Volodina S, Chaturvedi R, Lee KJ, Benson LN. Three-dimensional rotational angiography in the assessment of vascular and airway compression in children after a cavopulmonary anastomosis. *Pediatr Cardiol* 2015; 36: 1083–1089.
15. Aldoss O, Fonseca BM, Truong UT, et al. Diagnostic utility of three-dimensional rotational angiography in congenital cardiac catheterization. *Pediatr Cardiol* 2016; 37: 1211–1221.
16. Fagan T, Kay J, Carroll J, Neubauer A. 3-D guidance of complex pulmonary artery stent placement using reconstructed rotational angiography with live overlay. *Catheter Cardiovasc Interv* 2012; 79: 414–421.
17. Glockler M, Halbfabeta J, Koch A, Achenbach S, Dittrich S. Multimodality 3D-roadmap for cardiovascular interventions in congenital heart disease—a single-center, retrospective analysis of 78 cases. *Catheter Cardiovasc Interv* 2013; 82: 436–442.
18. Hill J, Bellotti C, Golden A. Three-dimensional rotational angiography during percutaneous device closure of Fontan fenestration. *World J Pediatr Congenit Heart Surg* 2013; 4: 324–325.
19. Poterucha JT, Foley TA, Taggart NW. Percutaneous pulmonary valve implantation in a native outflow tract: 3-dimensional DynaCT rotational angiographic reconstruction and 3-dimensional printed model. *JACC Cardiovasc Interv* 2014; 7: e151–152.
20. Anderson JH, Fetterly KA, Taggart NW. Three-dimensional rotational angiography-guided stent placement for treatment of acquired supravalvular aortic stenosis. *Circulation* 2015; 132: 455–456.
21. Stenger A, Dittrich S, Glockler M. Three-dimensional rotational angiography in the pediatric cath lab: optimizing aortic interventions. *Pediatr Cardiol* 2016; 37: 528–536.
22. Starmans NL, Krings GJ, Molenschot MM, van der Stelt F, Breur JM. Three-dimensional rotational angiography in children with an aortic coarctation. *Neth Heart J* 2016; 24: 666–674.
23. Goreczny S, Morgan GJ, Dryzek P, Moll JA, Moszura T. Initial experience with live three-dimensional image overlay for ductal stenting in hypoplastic left heart syndrome. *EuroIntervention* 2016; 12: 1527–1533.
24. Pockett CR, Moore JW, El-Said HG. Three dimensional rotational angiography for assessment of coronary arteries during melody valve implantation: introducing a technique that may improve outcomes. *Neth Heart J* 2017; 25: 82–90.
25. van der Stelt F, Krings GJ, Molenschot MC, Breur JM. Additional value of three-dimensional rotational angiography in the diagnostic evaluation and percutaneous treatment of children with univentricular hearts. *EuroIntervention* 2018; 14: 637–644.
26. Struffert T, Hauer M, Banckwitz R, Köhler C, Royalty K, Doerfler A. Effective dose to patient measurements in flat-detector and multislice computed tomography: a comparison of applications in neuroradiology. *Eur Radiol* 2014; 24: 1257–1265.
27. Parimi M, Buelter J, Thanugundla V, et al. Feasibility and validity of printing 3D heart models from rotational angiography. *Pediatr Cardiol* 2018; 39: 653–658.
28. Witowski J, Wake N, Grochowska A, et al. Investigating accuracy of 3D printed liver models with computed tomography. *Quant Imaging Med Surg* 2019; 9: 43–52.
29. Cignoni P, Rocchini C, Scopigno R. Metro: measuring error on simplified surfaces. *Comput Graph Forum* 1998; 17: 167–174.
30. Batteux C, Haidar MA, Bonnet D. 3D-printed models for surgical planning in complex congenital heart diseases: a systematic review. *Front Pediatr* 2019; 7: 23.
31. Kerrien E, Yureidini A, Dequidt J, Duriez C, Anxionnat R, Cotin S. Blood vessel modeling for interactive simulation of interventional neuroradiology procedures. *Med Image Anal* 2017; 35: 685–698.
32. Guo XY, He ZQ, Duan H, et al. The utility of 3-dimensional-printed models for skull base meningioma surgery. *Ann Transl Med* 2020; 8: 370.
33. Boyer PJ, Yell JA, Andrews JG, Seckeler MD. Anxiety reduction after pre-procedure meetings in patients with CHD. *Cardiol Young* 2020; 30: 997–994.
34. Sullivan PM, Liou A, Takao C, et al. Tailoring stents to fit the anatomy of unique vascular stenoses in congenital heart disease. *Catheter Cardiovasc Interv* 2017; 90: 963–971.
35. Zablah JE, Morgan GJ. Pulmonary artery stenting. *Interv Cardiol Clin* 2019; 8: 33–46.
36. Haddad L, Waller BR, Johnson J, et al. Radiation protocol for three-dimensional rotational angiography to limit procedural radiation exposure in the pediatric cardiac catheterization lab. *Congenit Heart Dis* 2016; 11: 637–646.